Optimization of the dynamic regulation in a branch-in metabolic pathway ⋆

Y. Boada * **F. N. Santos-Navarro** * **A. Vignoni** * **J. Picó** *

* *Synthetic Biology and Biosystems Control Lab, I.U. de Automática e Informática Industrial (ai2), Universitat Politècnica de Valencia, 46022, Camino de Vera S/N, Valencia, Spain.*
(e-mail: {yaboa,fersann1,alvig2,jpico}@upv.es)

Abstract: Multiobjective optimization has already been shown to be an appropriate tool to characterize and tune systems subject to multiple trade-offs among competing objectives. Here, we consider the dynamic regulation of a merging metabolic pathway motif. This motif appears in a wide range of metabolic engineering applications, including the production of phenylpropanoids highly appreciated by the pharma, nutraceutical and the cosmetic industries. We present an approach to use multiobjective optimization for the optimal tuning of the gene circuit parts composing the biomolecular controller and biosensor in the dynamic regulation of the metabolic pathway. We show how this approach can deal with the trade-offs between performance of the regulated pathway, robustness with respect to perturbations, and stability of the feedback loop. Our results suggest that the strategies for fine-tuning the trade-offs among performance, robustness, and stability in dynamic pathway regulation are complex and it is not always possible to infer them by simple inspection. This renders the use of the multiobjective optimization methodology not only useful but necessary.

Keywords: Synthetic biology; gene circuits; metabolic pathways; multiobjective optimization; dynamic regulation

1. INTRODUCTION

Metabolic engineering often seeks to obtain high levels of products of interest through genetic modification of microorganisms. That is, using microbial cell as an optimized factory. Natural cells use complex regulatory networks to preserve robust growth and endure environmental changes by dynamically adapting cell metabolism (Liu et al., 2018). These regulation strategies are the long-term result of evolution and in most cases they are not compatible with the addition of exogenous genes highly expressed to reach the production levels demanded by the industry.

Optimization methods like eg. Flux Balance Analysis (FBA), that make use of mathematical models of metabolism with only stoichiometric information and some basic regulatory information, have proved very valuable in predicting how cells adapt their metabolism according to different environmental conditions. These methods provide information on maximum theoretical yields, optimal flux distribution to maximize the flux towards some metabolite reaction bottlenecks, and required ways of intervention on gene expression leading to fluxes towards final products that achieve specified levels in productivity, titer and yield (Otero-Muras and Carbonell, 2021). This approach seeks the careful optimal selection of the constant expression levels for both the exogenous genes in the pathway of interest and the endogenous ones with relevant interactions. Yet, being a static regulation approach, it fails to address the dynamic and highly uncertain nature of the problem. Indeed, the static strategy to regulate a metabolic pathway relies on an optimization process that is tailor made for a particular situation. Therefore, it is not able to respond to cell and environmental changes occurring during fermentation in a bioreactor (Wehrs et al., 2019).

Achieving robust optimal production in microbial cell factories requires considering dynamic regulation of the pathway of interest. Dynamic feedback regulation is a very interesting strategy to construct pathways with the ability to self-tune upon changing environmental conditions and to overcome many of the ongoing challenges faced in metabolic engineering (Liu and Zhang, 2018; Hartline et al., 2020). For instance, finding the right enzyme levels that maximize production while avoiding pathway bottlenecks or accumulation of toxic intermediates is often a challenge. Feedback regulation circuits can address these problems by dynamically changing enzyme expression in response to metabolic inputs and continuously regulating the activity in the pathway in response to either intracellular or bioreactor perturbations. This will enable industry to attain higher process performance indices as compared to static regulation (Stevens and Carothers, 2015) and can lead to robust and efficient microbial production at the industrial level (Liu et al., 2018; Segall-Shapiro et al., 2018).

Despite the growing number of reported successful cases, engineering dynamic control strategies in biological applications remains a major challenge (Gao et al., 2019). There are algorithms that simulate and analyze the dynamic of complex metabolic networks using multi-objective optimal control prin-

⋆ This work was partially funded by by Grant MINECO/AEI, EU DPI2017-82896-C2-1-R and MCIN/AEI/10.13039/501100011033 grant number PID2020-117271RB-C21. YB thanks to Secretaría de Educación Superior, Ciencia, Tecnología e Innovación-Ecuador (Scholarship Convocatoria Abierta 2011) and Universitat Politècnica de València (Grant PAID-10-21 Acceso al Sistema Español de Ciencia e Innovación). F.N. Santos-Navarro is grateful to grant PAID-01-2017 (Universitat Politècnica de València)

ciples (Tsiantis and Banga, 2020). Yet, there are not generally applicable algorithms for designing dynamic metabolic regulation systems. The regulation topology is generally pathway-specific, depending both on the potential presence of toxic pathway intermediates and the pathway topology (Hartline et al., 2020). Several typical metabolic topology motifs are usually considered: linear, branched and merging (Blair et al., 2012). Most existing work has dealt with the dynamic regulation of linear pathways (Oyarzún and Stan, 2013; Liu and Zhang, 2018) or branched ones (Liu et al., 2018).

Here we consider the dynamic regulation of a branch-in from a metabolic pathway. In this metabolic motif, two substrates, a main precursor and an essential metabolite, are converted to an intermediate product which is subsequently transformed into a target product. In many practical situations, the secondary essential metabolite plays additional roles in the cell metabolism. Therefore, it is subject to environmentally-induced fluctuations. Over-expressing the enzyme that synthesizes this secondary metabolite or redirecting the flux towards it is not a feasible solution in cases where its accumulation is toxic for the cell, leading to growth inhibition.

Multi-objective optimization has already demonstrated to be an appropriate tool for characterization of gene circuit parts (Boada et al., 2019b,a), and for the design of gene circuits with a desired behavior (Boada et al., 2016, 2017, 2021). Here, we used multi-objective optimization for the optimal tuning of the gene circuit parts composing the biocontroller and biosensor in a dynamic metabolic regulation feedback loop. We show how this approach can deal with the trade-offs between performance of the regulated pathway and robustness with respect to fluctuations in the secondary metabolite. We highlight that performance indices must include not only the standard steady state industrial ones (eg. titer), but also indices related to the time-response transient (ie. stability). As the complexity of the dynamic biocontrollers and biosensors integrated in the feedback loop regulation increases, the stability and transient performance issues that high order dynamics introduce must be taken into account. We considered the case where having transcription factor (TF) based biosensors for producing the target product is not always possible. Alternatively, extended TF-based biosensors can be used. These introduce an additional pathway from the target product to be regulated to another measurable metabolite (Boada et al., 2020). Yet, these extended biosensors introduce extra dynamics in the feedback loop. To regulate the enzyme level that catalyses the conversion of the two substrates into the product, we considered the use of the antithetic controller, a biomolecular integral feedback controller that achieves quasi-perfect adaptation (Briat et al., 2016; Aoki et al., 2019).

We demonstrate our approach by a simple illustrative pathway that captures the essential topological features of merging metabolic pathways (Fig. 1A). We designed a feedback regulation strategy encompassing a simple TF-based biosensor to obtain readouts of the product and a simplified model of the biomolecular antithetic controller. The final titer of the target product and robustness with respect to fluctuations in the secondary metabolite are evaluated. We use a realistic model of the antithetic controller previously introduced in (Boada et al., 2020). The extra dynamics introduced by the biocontroller force us to take into account the transient dynamics of the regulated feedback loop in the design process. A library of designs is obtained, each one corresponding to a different trade-off. Our results suggest that the strategies for fine-tuning the trade-off between performance, robustness and stability in dynamic pathway regulation are complex, not being possible to obtain a solution by simple inspection. This renders the use of the multiobjective optimization methodology not only useful but necessary.

2. MATERIALS AND METHODS

2.1 Dynamic regulation of a branch-in metabolic pathway

To illustrate the broad scope and usefulness of our approach, we study a branch-in pathway with common features of a typical merging motif. Figure 1A depicts the production of a metabolite P from a precursor substrate S_1 and a secondary substrate S_2. The reaction is catalyzed by the enzyme E. This metabolic pathway can be described using the dynamic model in (1).

$$\begin{aligned}\frac{d[S_1]}{dt} &= V_{S_1} - V_{S_1,S_2} - \mu[S_1]\\ \frac{d[P]}{dt} &= V_{S_1,S_2} - \mu[P]\\ \frac{d[X]}{dt} &= \mu[X]\left(1 - \frac{[X]}{\mathrm{X_{max}}}\right)\end{aligned} \tag{1}$$

where $[S_i]$ and $[P]$ are the substrates and product concentrations. $[X]$ is the number of cells in the population. $[S_1]$ is the main substrate and $[S_2]$ the secondary substrate. The first order dilution term represents the effect of cell growth on the concentration of substrates and products, being μ the specific growth rate of the cell. $\mathrm{X_{max}}$ accounts for the maximum capacity of the population. The metabolic fluxes are given by the kinetic terms:

$$V_{S_1} = K_{S_1} \tag{2}$$

$$V_{S_1,S_2} = \mathrm{k_{cat}}[E]\frac{[S_1][S_2]}{\mathrm{K_{m12}} + \mathrm{K_{mS_2}}[S_1] + \mathrm{K_{mS_1}}[S_2] + [S_1][S_2]} \tag{3}$$

where we assumed that the uptake of the precursor S_1 has constant rate K_{S_1} (2), and the substrate S_2 is normally available at a non-limiting concentration. The flux V_{S_1,S_2} in Fig. 1A follows Michaelis-Menten kinetics, where $[E]$ is the concentration of the pathway enzyme, $\mathrm{k_{cat}}$ is the enzyme catalytic rate, $\mathrm{K_{mS_i}}$ are the Michaelis-Menten constants for the substrates, and $\mathrm{K_{m12}} = \mathrm{K_{mS_1}}\,\mathrm{K_{mS_2}}$. All the parameter values are listed in Table 1.

In the case of static pathway regulation (Fig. 2A, grey line), the flux V_{S_1,S_2} has a constant maximum value determined by the amount of the constitutively expressed heterologous enzyme E. As its expression level is independent of any metabolite in the pathway, the production of P is affected in the presence of a sudden change in the availability of the secondary substrate S_2 (right plot of Fig. 2A in dashed grey lines).

On the contrary, in the case of dynamic pathway regulation (Fig. 2A in orange line), the expression level of the enzyme E depends on the amount of the product metabolite. A biosensor provides product metabolite readouts and a biomolecular controller changes the enzyme expression level as a function of the difference between the current amount of product and the target one encoded in the controller. Thus, when there is a change in the substrate S_2 the production of the metabolite P is affected. Yet, it is able to recover (up to some extent) closer to its previous value (Fig. 2A, right plot, solid orange line).

Different control architectures can be implemented with combinations of activation and repression feedback loops. Here, we focus on a class of biomolecular controller, the antithetic controller Aoki et al. (2019), that allows for quasi-perfect adaptation. Figure 1B shows the antithetic controller regulating the amount of enzyme E using a simple TF-based biosensor to obtain readouts of P.

The control action is encoded by free σ molecules that activate the expression of the enzyme E through its promoter P_σ. We modeled the promoter using a generalized Hill function as in Boada et al. (2020), including the effect of the plasmid copy number $\mathrm{C_N}$ on the promoter activation function. The resulting dynamics of the enzyme E is:

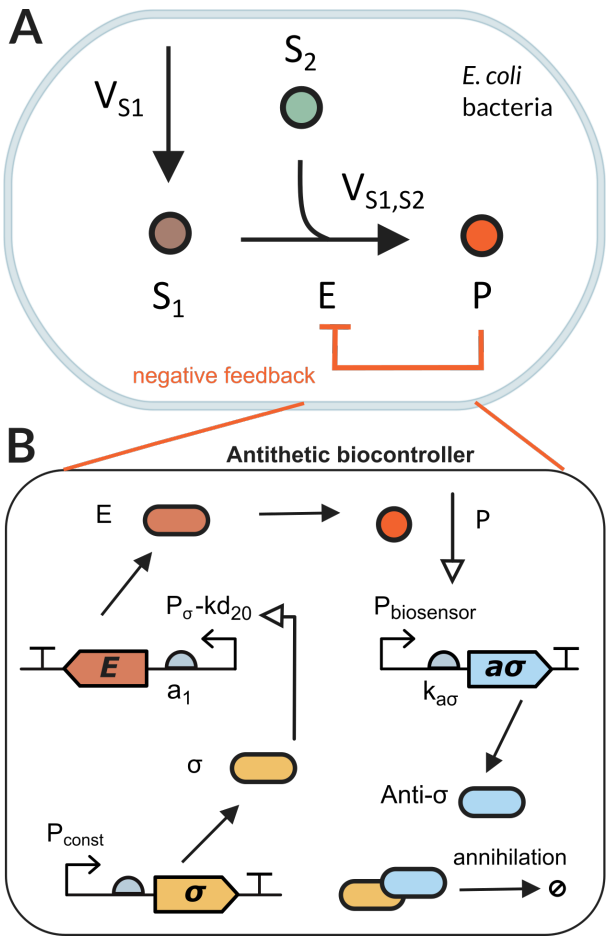

Fig. 1. **Illustrative model system. (A)** Metabolic pathway for production of the metabolite P. The main substrate S_1 and the secondary one S_2 are converted into the product P by the catalyst enzyme E. In the static regulation strategy (black lines) the expression level of the enzyme E remains constant in time. Conversely, in the dynamic regulation strategy (orange line), the expression of E depends on the amount of product P. **(B)** Biosensor and antithetic controller configuration for dynamic pathway regulation in bacteria. The amount of free σ molecules determine the expression of the enzyme E. A TF-based biosensor detects the product levels and counteracts expressing the anti-σ molecule. When P decreases, the controller reduces the amount of expressed anti-σ, therefore the free σ level rises up-regulating the enzyme.

Table 1. Model parameters values

Parameter	Description	Value
a_0	E constitutive expression	0.154 $\mathrm{min^{-1}}$
TF	Biosensor TF concentration	0.154 molec
$\mathrm{C_N}$	Plasmid copy number	10 copies
k_σ	Expression strength	10 $\mathrm{min^{-1}}$
$\mathrm{d_c}$	degradation rate $[\sigma \cdot a\sigma]$	1×10^{-3} $\mathrm{min^{-1}}$
$\mathrm{kd_P}$	dissociation constant TF to P	1.5×10^4 molec
γ	dissociation constant $[\sigma \cdot a\sigma]$	0.01 $\mathrm{molec^{-1}}$ $\mathrm{min^{-1}}$
d_σ, $\mathrm{d}_{a\sigma}$, $\mathrm{d_E}$	protein degradation rate	3×10^{-4} $\mathrm{min^{-1}}$
$\mathrm{k_{cat}}$	F3H catalytic constant	0.42 $\mathrm{min^{-1}}$
$\mathrm{K_{mS_1}}$	Michaelis constant $\mathrm{E-S_2}$	1e-3 molec
$\mathrm{K_{mS_2}}$	Michaelis constant $\mathrm{E-S_1}$	1e-3 molec

$$\frac{d[E]}{dt} = \mathrm{C_N}a_0 + \mathrm{C_N a_1}\frac{[\sigma]^2}{(\mathrm{k_{d20}C_N})^2 + [\sigma]^2} - (\mathrm{d_E} + \mu)\,[E] \tag{4}$$

with the parameter values in Table 1. The acting molecule σ is constitutively expressed (thus encoding for a sort of target set-point value) and binds the anti-σ molecule to form an inactive complex, effectively reducing the amount of free σ. The resulting dynamics of the free σ molecules is:

$$\frac{d[\sigma]}{dt} = \mathrm{C_N k}_\sigma - \gamma[\sigma][a\sigma] - (\mathrm{d}_\sigma + \mu)\,[\sigma] \tag{5}$$

where the parameter values are listed in Table 1. The dynamics of the anti-σ molecule is:

$$\frac{d[a\sigma]}{dt} = \mathrm{C_N k}_{a\sigma}\frac{\mathrm{C_N}^2\left(1+\frac{[P]}{\mathrm{k_{dp}}}\right)^2}{\mathrm{C_N}^2\left(1+\frac{[P]}{\mathrm{k_{dp}}}\right)^2 + [\mathrm{TF}]^2} - \gamma[\sigma][a\sigma] - (\mathrm{d}_{a\sigma} + \mu)\,[a\sigma] \tag{6}$$

Fig. 1B illustrates how the TF-based biosensor detects the product P and expresses the anti-σ molecule as a function of it. As the concentration of P decreases, so does the amount of expressed anti-σ. Thus, the amount of free σ increases, up-regulating the expression of the enzyme E.

The model in Eq. (4-6) shows how the dynamics of both TF-based biosensor and the antithetic biocontroller depend on their composing parts (see the gene circuit in Fig. 1B). We only tuned those parts which can be experimentally modified in the lab.

2.2 *Multi-objective optimization*

A multi-objective problem is often faced by building an aggregate function to assemble the objectives in a unique index or vector that contains a weight for each objective. However, the solution thus obtained is determined by the selection of these weighting values. An alternative option is to use a truly multi-objective optimization design where all objectives, equally important, are optimized simultaneously (Miettinen, 1999). Instead of one rarely unique solution, a set of the best solutions, known as *Pareto Front*, is obtained. All solutions in this front are *Pareto-optimal* and only differ from each other in the trade-off of objectives each one represents. Multi-objective optimization requires at least three fundamental steps (Miettinen et al., 2008): (1) the multi-objective problem definition (MOP), (2) the optimization process, and (3) the multi-criteria decision making process (MCDM). The overall multi-objective optimization design enables to analyze current trade-offs between the objectives and select the most suitable solutions (Reynoso-Meza et al., 2013).

Multi-objective problem definition. As in Miettinen et al. (2008), a Multi-objective Problem (MOP) can be stated as follows:

$$\min_{\theta} \mathbf{J}(\theta) = [J_1(\theta), ..., J_m(\theta)] \tag{7}$$

subject to:

$$\mathbf{K}(\theta) \leq 0$$
$$\underline{\theta_i} \leq \theta_i \leq \overline{\theta_i}, \ \ \forall i = [1, ..., n]$$

where $\mathbf{J}(\theta)$ is the objective vector, m is the number of objectives, $\theta = [\theta_1, \theta_2, ..., \theta_n]$ is the decision vector that contains the decision variables for multi-objective optimization; $\mathbf{K}(\theta)$ are the inequality and equality constraint vectors; $\underline{\theta_i}$, $\overline{\theta_i}$ are the lower and upper bounds in the decision variables space $\mathbf{\Theta}$. The MOP (7) has a set of solutions, the Pareto Set Θ_P, whose values in the Pareto front are a function of the decision variables. Each solution in this set corresponds to an optimal objective vector in the Pareto Front $\mathbf{J_P}$. All solutions in the the Pareto Set are Pareto-optimal non dominated solutions, that is, they differ from each other in the objectives trade-off each one represents.

3. RESULTS

3.1 MOP definition of the branch-in pathway

For the optimization process, we considered two objective functions to characterize the trade-offs between reaching a desired titer target for P while reducing the production loss after a perturbation on the level of the secondary metabolite S_2 (Fig. 2).

For the titer (J_1, left plot in Fig. 2A), we looked for the difference between the titer of the product P in the bioreactor and a desired target value. In other words, J_1 is the target titer error. For the production loss (J_2, right plot in Fig. 2A), we focused on the relative production loss (amount of product expressed per cell) after a perturbation on S_2. The corresponding expressions for both objectives to be jointly minimized are:

$$J_1 = |\text{Target} - K[P]_{\text{unperturbed}}(T)| \tag{8}$$
$$J_2 = \left| \frac{[P]_{\text{unperturbed}}(T) - [P]_{\text{perturbed}}(T)}{[P]_{\text{unperturbed}}(T)} \right| \tag{9}$$

where $[P]_{\text{unperturbed}}(T)$ is the product concentration at the end of the experiment (time T), K is a constant to convert into titer taking into account the growth of the culture and the molecular weight of the product P, $[P]_{\text{perturbed}}(T)$ is the product concentration after the perturbation in the secondary metabolite. As J_1 describes the difference between the desired target titer and the actual one, low values of J_1 imply an increased titer. On the other hand, J_2 is related to the loss in production after a perturbation. Therefore, small values of J_2 correspond to low production loss after a perturbation, that is, better rejection of the perturbation on the secondary metabolite.

We selected the following biosensor and biocontroller parameters to be tuned, considering they are accessible to be experimentally changed in the biological implementation of the system: expression strength for the enzyme E, $\mathrm{a_1}$; the dissociation constant between σ and the enzyme promoter, $\mathrm{k_{d20}}$; and the expression strength for anti-σ , $\mathrm{k_{a\sigma}}$. Additionally, the specific growth rate, μ, was included as decision parameter to account for the dependency of the results on cell growth and the subsequent dilution effect. Table 2 lists the biological bounds set for each decision variable.

Table 2. Bounds for the branch-in pathway MOP

Bound	$\mathrm{k_{a\sigma}}\,(\mathrm{min^{-1}})$	$\mathrm{k_{d20}}\,(\mathrm{molec})$	$\mathrm{a_1}\,(\mathrm{min^{-1}})$	$\mu\,(\mathrm{min^{-1}})$
Lower	700	100000	90	0.005
Upper	1500	350000	160	0.01

The goal is to obtain a library of possible designs, each one corresponding to a different trade-off between the cost indices J_1, J_2. The resulting solutions are all equally optimal in the sense of Pareto (Boada et al., 2019b). That is, when one of the objectives improves the others necessarily deteriorate, so that the selection of the most appropriate solution depends on the designer. Hence, the MOP can be stated as:

$$\min_{\theta \in \Re^4} \mathrm{J}(\theta) = [J_1(\theta), J_2(\theta)] \in \Re^2$$
$$\text{subject to :equations } (1-6)$$

We computed the values of the selected parameters as solutions for the multiobjective optimization problem $\min(J_1, J_2)$ subject to biologically plausible bounds on the values of the parameters. The optimization problem was solved using a genetic multiobjective optimization algorithm based on differential evolution.

3.2 MCDM: choosing a design from the library

The resulting Pareto front (Fig. 2B) has three distinct regimes: (i) large titer target error and low production loss, (ii) small titer target error and high production loss, and (iii) a best trade-off regime between the two competing objectives. The convexity of the Pareto front indicates that the optimization problem is well-posed, in the sense that both objective functions oppose each other across the whole space of optimal solutions. We selected five solutions that represent the mentioned regimes. These solutions are highlighted in the Pareto front in Fig. 2B. The objective values of the selected solutions are shown in Fig. 3A, and their corresponding tuned optimal values for the controller and biosensor parameters including the growth rate are depicted in Fig. 3B. Thus, the set of solutions of the optimization constitute a library of optimally tuned controller-biosensor pairs.

A detailed inspection of the library of the controller and biosensor pairs obtained (Fig. 3B) reveals that the relations between parameters and objectives are not necessarily monotonous. For example, the dissociation constant $\mathrm{k_{d20}}$ should be smaller in order to reduce the production loss after perturbation (J_2). Yet, there is no monotonous trend in neither the anti-σ expression strength $k_{a\sigma}$ nor in the E enzyme expression strength a_1.

Altogether these results suggest that strategies for fine-tuning the trade-off between target titer error and the production loss in dynamic pathway regulation are complex. Thus, it would not have been possible to obtain a set of parameters that simultaneously optimize the objectives by simple inspection or standard single- or lumped-objective optimization, even for this simplified case.

4. CONCLUSION

Dynamic regulation of metabolic pathways is a key strategy to achieve optimal production in microbial cell factories while coping with cell and environmental fluctuations. The appropriate dynamic regulation topology will be very specific to the

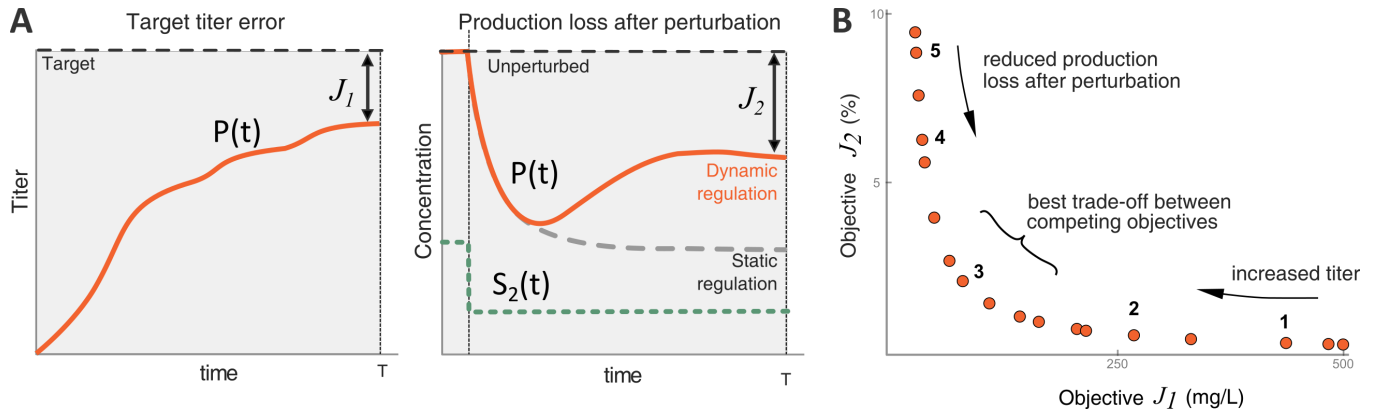

Fig. 2. **(A)** Objective functions defined for maximizing the production of P up to a target titer value (J_1) while minimizing the production loss after perturbations (J_2). **(B)** Pareto front with optimal solutions for the dynamical pathway regulation. Solutions on the right side have larger titer target error J_1 (*ie.* lower titer) and a small production loss after perturbation J_2 (*ie.* higher titer after the perturbation). Moving along the Pareto front towards the left, the titer target error decreases and the production loss increases. Solutions in the middle of the Pareto front have the best trade-off between the competing objectives J_1 and J_2.

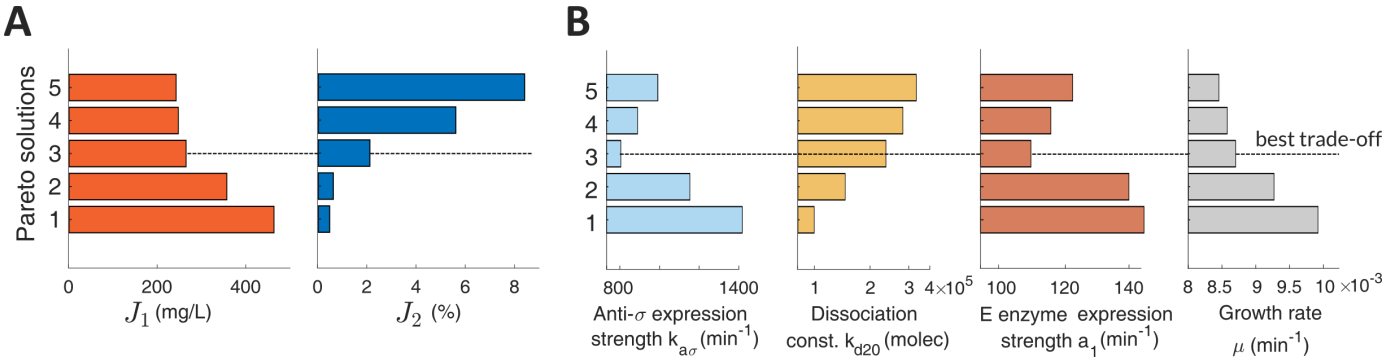

Fig. 3. **Pareto solutions**. Pareto front and Pareto set of selected solutions. **(A)** Pareto front showing the solutions of the multiobjective problem. The values of the objectives J_1 and J_2 (x-axis) are represented for different solutions (y-axis). **(B)** The Pareto set represented with a plot for each tuned parameter. The tuned values of the parameters (x-axis) are shown for each selected Pareto solution (y-axis). The set of solutions constitutes the library of biocontrollers and biosensors obtained with the multiobjective optimization tuning process.

topology and characteristics of the metabolic pathway to be regulated. Yet, some basic metabolic motifs that often appear in practical industrial applications and their appropriate dynamic regulation topology can be identified. In addition, all dynamic regulation schemes share a set of common features that determine to great extent the appropriate methodological tools required for the optimal selection of the gene circuit parts composing them. In particular, there is the common need to address a set of multiple goals related to the performance of the system, in terms of both the production of the targeted product and the rejection of perturbations affecting it. Moreover, the stability issues that arise as result of using feedback regulation strategies must be addressed. This is even more important as we use complex biomolecular controllers and metabolic extended biosensors that introduce extra dynamics that may compromise the transient time response and stability of the regulated system.

Here we have shown a general approach using multi-objective model-based optimization for building libraries of gene circuit parts that achieve optimal performance of a dynamically regulated merging metabolic pathway. This metabolic motif appears in many situations of practical interest. In particular, this is a pervasive motif in the pathways of phenylpropanoid-derived natural products. In this case, the multi-objective optimization approach obtains devices within the resulting libraries that can have different combinations of parameter values but similar performances in the Pareto sense. This is a sign of the inherent robustness obtained with negative feedback control. Interestingly, depending on the available biological parts, one implementation can be more feasible than another one, increasing the importance of having such variety of elements in the library.

Our results show the importance of design models considering the metabolic kinetics together with the biosensor and biocontroller dynamics with enough degree of granularity. Not only they better assist in the *in vivo* implementation of the system as compared to coarse-grain models, but also force to take into account the transient and stability issues often disregarded.

The need of sufficiently detailed models arguably includes the use of host-aware models. Indeed, the library of designs obtained might suffer some modifications, in case we considered the interactions between the regulated metabolic pathway and the host cell caused by competition for cell resources (Santos-Navarro et al., 2021). Our goal here was to present the general multi-objective optimization approach, with emphasis on the tuning of the biomolecular controller and biosensor. The ad-

ditional use of host-aware models will not change the general framework.

Altogether our results suggest that strategies for fine-tuning the trade-offs among target performance, robustness and stability in complex dynamic pathway regulation topologies are intricate and impossible to obtain by simple inspection. This suggests the multi-objective optimization methodology as an useful and necessary tool to fulfill all trade-offs. As a consequence, it will not be generally possible to obtain widely applicable optimal simple design guidelines that can assist in the *in vivo* implementation. Instead, the expected outcome of the tuning process should be libraries of gene circuit components that achieve specific trade-offs for specific nominal environmental situations.

REFERENCES

Aoki, S.K., Lillacci, G., Gupta, A., Baumschlager, A., Schweingruber, D., and Khammash, M. (2019). A universal biomolecular integral feedback controller for robust perfect adaptation. *Nature*, 570(7762), 533–537. doi:10.1038/s41586-019-1321-1. URL http://www.nature.com/articles/s41586-019-1321-1.

Blair, R.H., Kliebenstein, D.J., and Churchill, G.A. (2012). What can causal networks tell us about metabolic pathways? *PLoS Computational Biology*, 8(4). doi:10.1371/journal.pcbi.1002458.

Boada, Y., Vignoni, A., Alarcon-Ruiz, I., Andreu-Vilarroig, C., Monfort-Llorens, R., Requena, A., and Picó, J. (2019a). Characterization of Gene Circuit Parts Based on Multiobjective Optimization by Using Standard Calibrated Measurements. *ChemBioChem*, 20(20). doi:10.1002/cbic.201900272.

Boada, Y., Vignoni, A., and Picó, J. (2017). Multi-objective optimization for gene expression noise reduction in a synthetic gene circuit. *IFAC-PapersOnLine*, 50(1), 4472 – 4477. 20th IFAC World Congress.

Boada, Y., Picó, J., and Vignoni, A. (2021). *Multi-objective optimization tuning framework for kinetic parameter selection and estimation*. Methods in Molecular Biology, vol 2385. Springer US, New York, NY. doi:10.1007/978-1-0716-1767-0.

Boada, Y., Reynoso-Meza, G., Picó, J., and Vignoni, A. (2016). Multi-objective optimization framework to obtain model-based guidelines for tuning biological synthetic devices: an adaptive network case. *BMC systems biology*, 10(1), 27. doi:10.1186/s12918-016-0269-0.

Boada, Y., Vignoni, A., and Picó, J. (2019b). Multiobjective identification of a feedback synthetic gene circuit. *IEEE Transactions on Control Systems Technology*, 28(1), 208–223. doi:10.1109/TCST.2018.2885694.

Boada, Y., Vignoni, A., Picó, J., and Carbonell, P. (2020). Extended Metabolic Biosensor Design for Dynamic Pathway Regulation of Cell Factories. *iScience*, 23(7). doi:10.1016/j.isci.2020.101305.

Briat, C., Gupta, A., and Khammash, M. (2016). Antithetic Integral Feedback Ensures Robust Perfect Adaptation in Noisy Bimolecular Networks. *Cell Systems*, 2(1), 15–26. doi:10.1016/j.cels.2016.01.004. URL http://dx.doi.org/10.1016/j.cels.2016.01.004.

Gao, C., Xu, P., Ye, C., Chen, X., and Liu, L. (2019). Genetic Circuit-Assisted Smart Microbial Engineering. *Trends in Microbiology*. doi:10.1016/j.tim.2019.07.005. URL https://linkinghub.elsevier.com/retrieve/pii/S0966842X19301866.

Hartline, C.J., Schmitz, A.C., Han, Y., and Zhang, F. (2020). Dynamic control in metabolic engineering: Theories, tools, and applications. *Metabolic Engineering*, (July). doi:10.1016/j.ymben.2020.08.015. URL https://doi.org/10.1016/j.ymben.2020.08.015.

Liu, D., Mannan, A.A., Han, Y., Oyarzún, D.A., and Zhang, F. (2018). Dynamic metabolic control: towards precision engineering of metabolism. *Journal of Industrial Microbiology Biotechnology*, 45(7), 535–543. doi:10.1007/s10295-018-2013-9. URL https://academic.oup.com/jimb/article/45/7/535-543/5996684.

Liu, D. and Zhang, F. (2018). Metabolic Feedback Circuits Provide Rapid Control of Metabolite Dynamics. *ACS Synthetic Biology*, 7(2), 347–356. doi:10.1021/acssynbio.7b00342. URL https://pubs.acs.org/doi/abs/10.1021/acssynbio.7b00342.

Miettinen, K. (1999). *Nonlinear Multiobjective Optimization*, volume 12. Kluwer Academic Publishers, Boston.

Miettinen, K., Ruiz, F., and Wierzbicki, A.P. (2008). Introduction to multiobjective optimization: interactive approaches. In *Multiobjective Optimization*, 27–57. Springer.

Otero-Muras, I. and Carbonell, P. (2021). Automated engineering of synthetic metabolic pathways for efficient biomanufacturing. doi:10.1016/j.ymben.2020.11.012.

Oyarzún, D.A. and Stan, G.B.V. (2013). Synthetic gene circuits for metabolic control: design trade-offs and constraints. *Journal of The Royal Society Interface*, 10(78), 20120671. doi:10.1098/rsif.2012.0671. URL https://royalsocietypublishing.org/doi/10.1098/rsif.2012.0671.

Reynoso-Meza, G., García-Nieto, S., Sanchis, J., and Blasco, X. (2013). Controller tuning using multiobjective optimization algorithms: a global tuning framework. *IEEE Transactions on Control Systems Technology*, 21(2), 445–458.

Santos-Navarro, F.N., Boada, Y., Vignoni, A., and Picó, J. (2021). Rbs and promoter strengths determine the cell growth-dependent protein mass fractions and their optimal synthesis rates. *ACS synthetic biology*. doi:10.1021/acssynbio.1c00131.

Segall-Shapiro, T.H., Sontag, E.D., and Voigt, C.A. (2018). Engineered promoters enable constant gene expression at any copy number in bacteria. *Nature Biotechnology*, 36(4), 352–358. doi:10.1038/nbt.4111. URL https://doi.org/10.1038%2Fnbt.4111.

Stevens, J.T. and Carothers, J.M. (2015). Designing RNA-Based Genetic Control Systems for Efficient Production from Engineered Metabolic Pathways. *ACS Synthetic Biology*, 4(2), 107–115. doi:10.1021/sb400201u. URL http://pubs.acs.org/doi/10.1021/sb400201u.

Tsiantis, N. and Banga, J.R. (2020). Using optimal control to understand complex metabolic pathways. *BMC Bioinformatics*, 21(1), 472. doi:10.1186/s12859-020-03808-8. URL https://doi.org/10.1186/s12859-020-03808-8.

Wehrs, M., Tanjore, D., Eng, T., Lievense, J., Pray, T.R., and Mukhopadhyay, A. (2019). Engineering Robust Production Microbes for Large-Scale Cultivation. *Trends in Microbiology*, 27(6), 524–537. doi:10.1016/j.tim.2019.01.006.